Plant Molecular Biology (2021) 107:37–48
https://doi.org/10.1007/s11103-021-01176-2

Structural insights into the allosteric site of Arabidopsis NADP-malic enzyme 2: role of the second sphere residues in the regulatory signal transmission

Mariel Claudia Gerrard Wheeler[1] · Cintia Lucía Arias[1] · Juliana da Fonseca Rezende e Mello[2] · Nuria Cirauqui Diaz[2] · Carlos Rangel Rodrigues[2] · María Fabiana Drincovich[1] · Alessandra Mendonça Teles de Souza[2] · Clarisa Ester Alvarez[1]

Received: 19 February 2021 / Accepted: 22 July 2021 / Published online: 31 July 2021

Abstract

Key message **NADP-ME2 from *Arabidopsis thaliana* exhibits a distinctive and complex regulation by fumarate, acting as an activator or an inhibitor according to substrate and effector concentrations. In this work, we used molecular modeling approach and site-directed mutagenesis to characterized the NADP-ME2 structural determinants necessary for allosteric regulation providing new insights for enzyme optimization.**

Abstract Structure–function studies contribute to deciphering how small modifications in the primary structure could introduce desirable characteristics into enzymes without affecting its overall functioning. Malic enzymes (ME) are ubiquitous and responsible for a wide variety of functions. The availability of a high number of ME crystal structures from different species facilitates comparisons between sequence and structure. Specifically, the structural determinants necessary for fumarate allosteric regulation of ME has been of particular interest. NADP-ME2 from *Arabidopsis thaliana* exhibits a distinctive and complex regulation by fumarate, acting as an activator or an inhibitor according to substrate and effector concentrations. However, the 3D structure for this enzyme is not yet reported. In this work, we characterized the NADP-ME2 allosteric site by structural modeling, molecular docking, normal mode analysis and mutagenesis. The regulatory site model and its docking analysis suggested that other C4 acids including malate, NADP-ME2 substrate, could also fit into fumarate's pocket. Besides, a non-conserved cluster of hydrophobic residues in the second sphere of the allosteric site was identified. The substitution of one of those residues, L62, by a less flexible residue as tryptophan, resulted in a complete loss of fumarate activation and a reduction of substrate affinities for the active site. In addition, normal mode analysis indicated that conformational changes leading to the activation could originate in the region surrounding L62, extending through the allosteric site till the active site. Finally, the results in this work contribute to the understanding of structural determinants necessary for allosteric regulation providing new insights for enzyme optimization.

Mariel Claudia Gerrard Wheeler and Cintia Lucía Arias have contributed equally to this work.

✉ Alessandra Mendonça Teles de Souza
amtsouza@pharma.ufrj.br

✉ Clarisa Ester Alvarez
alvarez@cefobi-conicet.gov.ar

[1] Centro de Estudios Fotosintéticos y Bioquímicos, Facultad de Ciencias Bioquímicas y Farmacéuticas, Universidad Nacional de Rosario (CEFOBI-CONICET-UNR), Suipacha 570, Rosario, Argentina

[2] Faculdade de Farmácia, Laboratório de Modelagem Molecular & QSAR (ModMolQSAR), Universidade Federal do Rio de Janeiro, Av. Carlos Chagas Filho, 373 bloco L subsolo, Cidade Universitária, Rio de Janeiro, Brazil

Graphic abstract

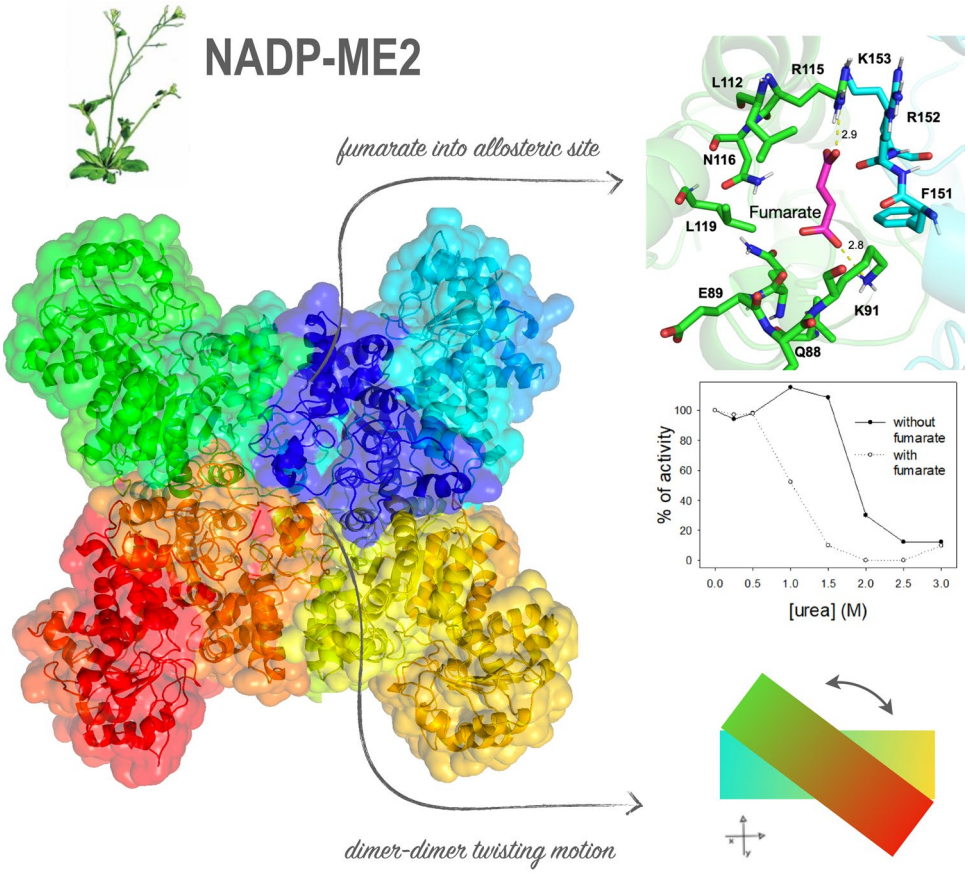

Keywords Malic enzyme · Fumarate regulation · Structure–function

Introduction

The widely distributed malic enzyme (ME) participates in different biological functions as diverse as lipogenesis, photosynthesis and organic acid metabolism. In the presence of a divalent cation, this enzyme catalyzes the oxidative decarboxylation of malate to pyruvate, NAD(P)H, and CO_2. MEs of a number of sources including humans, pigeons, nematodes, bacteria, phytopathogens and plants have been kinetically and structurally characterized. Currently, there are around 30 crystal structures of MEs uploaded in the Protein Data Bank (Xu et al. 1999; Coleman et al. 2002; Yang et al. 2002a, b; Chang and Tong 2003; Rao et al. 2003; Alvarez et al. 2018, 2019). Besides significant sequence homology, all eukaryotic ME structures present an overall similar tetrameric aggrupation as dimer of dimers, with a global conservation of the structural domains in each of their monomers. However, distinctive intrinsic characteristics associated with regulatory sites were also described. Almost 50% of the known structures correspond to the human mitochondrial isoform using both NAD or NADP as cofactor (HsmNAD(P)-ME), of which several were designed to analyze effector binding mechanisms. Specifically for fumarate it has been identified the presence of an allosteric binding site and essential residues (R67, E69, R91 and D102) involved in the regulation (Yang et al. 2002a; Hung et al. 2005; Hsieh et al. 2009b, 2019).

In plants, MEs are present as larger gene families with members in mitochondria, plastids, and cytosol of different tissues and organs (Drincovich et al. 2010). They play important roles in controlling the highly changeable levels of organic acids, reduced cofactors, and CO_2 in processes including photosynthesis, respiration, protein and lipid biosynthesis, pH regulation, and defense responses (Brown et al. 2010; Voll et al. 2012; Maurino and Engqvist 2015; Tronconi et al. 2018; Alvarez et al. 2019). Particularly, the model plant *Arabidopsis thaliana* accumulates malate and fumarate at variable levels according to day-night cycle, organ, developmental stage and growing conditions (Fernie and Martinoia 2009; Araújo et al. 2011). Within its ME

isoforms, Arabidopsis cytosolic NADP-ME2 presents a constitutive expression, the highest catalytic activity and it is the most regulated by cellular metabolites (Gerrard Wheeler et al. 2005, 2008). NADP-ME2 has been found to be specifically activated by succinate, fumarate, aspartate and CoA (Gerrard Wheeler et al. 2008, 2009). Especially fumarate regulation in this enzyme follows a complex mechanism not described in any other ME. This modulator can act as an allosteric activator or a competitive inhibitor depending on its own concentration, substrate levels and pH, as well as, affect the reverse reaction (Arias et al. 2013; Badia et al. 2017). Our previous studies showed that the residue R115 (R91, in HsmNAD(P)-ME) is necessary for NADP-ME2 activation (Gerrard Wheeler et al. 2008). However, not all the residues described as essential for the regulation in the human enzyme are present in NADP-ME2. These differences, together with the distinctive kinetic behavior, suggest that the structural determinants for the regulatory mechanism must present contrasting points between both isoenzymes. Thus, in this work, we performed a comprehensive analysis of the fumarate allosteric site in NADP-ME2 by in silico analysis and site-directed mutagenesis. The results obtained revealed the participation of the N-terminal region of NADP-ME2, specifically the residue L62, in fumarate regulation. Furthermore, this work provides evidence that suggests that this region would be responsible for transmitting the regulatory signal to the active sites in NADP-ME2. Finally, these results contribute to a better understanding of a regulatory mechanism and could facilitate enzyme design and engineering.

Materials and methods

Structural models of NADP-ME2 proteins

Three-dimensional (3D) models of native Arabidopsis NADP-ME2 plus ME2-R115A and ME2-L62W mutant versions were obtained by a combination of comparative and de novo modeling. The amino acid sequence of the enzyme was retrieved from UniProtKB (ID Q9LYG3). Template structure was obtained by searching ME isoforms crystallized in the presence of fumarate against Protein Data Bank (PDB, (Berman et al. 2000)). The 3D models were constructed using Modeller program v9.13 (Šali and Blundell 1993). The N-terminal was constructed using the I-TASSER server (Yang and Zhang 2015). A total of 100 models were generated, and the model with the best DOPE score was selected. The overall stereochemical quality of the developed models was assessed using PROCHECK (Laskowski et al. 1993). The NADP-ME2 modeled structure was uploaded at the Protein Molecular Data Base (PMDB id: PM0083497).

Molecular docking

Molecular docking between the enzymes and ligands were performed using AutoDock 4.2 (Morris et al. 2009). The protein protonation state at pH 7.4 was obtained from PDB2PQR server (Dolinsky et al. 2004) and the Gasteiger charges were calculated with AutoDock tools (Morris et al. 2009). The structures of fumarate and malate at pH 7.4 were downloaded from ZINC database. Each geometry was optimized with Ghemical software and the atomic charges were added using the parameterization AM1-BCC of the UCSF Chimera system (Pettersen et al. 2004). The best parameters were set up by re-docking using the HsmNAD(P)-ME complexed with malate and fumarate (PDB ID 1PJ2, resolution 2.3 Å). A docking grid of $30 \times 46 \times 34$ points centered on the allosteric site was used for 100 runs of the genetic algorithm, where the best score was selected. Different backbone-dependent rotamers for L62, K91, R115 and R152 amino acids were created and the ligand was docked on each new structure.

Normal mode analysis

Normal mode analysis of NADP-ME2 was performed by the anisotropic network model (Eyal et al. 2015) with ProDy software (Bakan et al. 2011). The results were visualized using the VMD program (Humphrey et al. 1996). The hinge regions (flexible joints) were calculated by Bio3d (Grant et al. 2006) as the regions of minimal mean square fluctuations for a given mode.

Expression and purification of recombinant ME2-L62W

Site-directed mutagenesis of NADP-ME2 was carried out following the protocol previously described in (Detarsio et al. 2003). Briefly, the pET32a plasmid containing NADP-ME2 cDNA (Gerrard Wheeler et al. 2005) was used as PCR template together with the primer: 5′ CAGTAAACGCCC ATCCCTTGTTG 3′ that allows the introduction of the desired mutation in the amplified fragment (L62W). The product was sequenced (Macrogen) to confirm the presence of the correct sequence change. ME2-L62W was expressed merged in frame to a His-tag to allow the purification by a nickel-containing His-bind column (Novagen), as parental NADP-ME2 and ME2-R115A mutant (Gerrard Wheeler et al. 2005, 2008; Arias et al. 2013). The purified enzymes were concentrated on Centricon YM-50 (Millipore), analyzed by SDS-PAGE to verify integrity and purity and stored at -80 °C in 100 mM Tris–HCl pH 7.5, 10 mM $MgCl_2$ and 10% (v/v) glycerol for further studies.

Gel electrophoresis

SDS-PAGE was performed in 10% (w/v) polyacrylamide gels as described in Laemmli, 1970. Then, the proteins were visualized with Coomassie blue.

Native-PAGE was performed using a 6% (w/v) acrylamide separating gel. Electrophoresis was run at 150 V at 10 °C. Proteins were then assayed for NADP-ME activity by incubating in a solution containing the reaction substrates plus 35 µg/ml nitroblue tetrazolium and 0.85 µg/ml phenazine methosulfate a 30 °C.

Gel filtration chromatography

The protein native molecular mass was also evaluated by gel filtration chromatography on an ÄKTA purifier system (GE Healthcare) using a Tricorn Superdex 200 10/300 GL (GE Healthcare). The column was equilibrated with 50 mM Tris–HCl at pH 7.5 and calibrated using molecular mass standards (29–443 kDa; Sigma Aldrich). Each protein was applied separately in a final volume of 100 µl at a constant flow rate of 0.5 ml/min.

Circular dichroism assays

Circular dichroism spectra were obtained using 30 µg of proteins on a Jasco J-810 spectropolarimeter averaging 10 scans between 200 and 250 nm. Mean amino acid residue ellipticity was calculated according to (Detarsio et al. 2003).

Activity assays and protein concentration measurement

NADP-ME activity assays were performed at 30 °C in a Jasco V-730 spectrophotometer using a reaction mixture containing 100 mM Tris–HCl pH 7.5, 10 mM $MgCl_2$ and variable concentrations of NADP (0–9 mM) and malate (0–70 mM). One unit (U) is defined as the amount of enzyme that catalyzes the formation of 1 µmol of NADPH min^{-1} under the specified conditions ($\varepsilon_{340nm} = 6.22\ mM^{-1}\ cm^{-1}$). Kinetic parameters were calculated by triplicate determinations fitting the data to the Hill equation. NADP-ME activity was also measured in the presence of different fumarate concentrations (up to 25 mM). To avoid changing the pH, malate and fumarate solutions brought to pH 7.5 were used. Protein concentration was determined by the BioRad protein assay using total serum proteins as standard.

Urea denaturation experiments

Each protein was pre-incubated for 30 min at 0 °C in the absence or presence of 20 mM fumarate. Then, the samples were exposed to different concentrations of urea (0–3 M) for 30 min at 25 °C. Finally, the enzyme denaturation was quantified by NADP-ME activity determination as described above.

Fluorescence quenching of the tryptophan residues

Fluorescence data were collected in a Cary Eclipse fluorescence spectrophotometer. The excitation wavelength was set to 295 nm to selectively excite tryptophan residues of the proteins. The quenching was carried out by sequentially adding small volumes of malate solution to each enzyme. The recorded values were corrected by buffer fluorescence and dilution, and represented using the modified Stern–Volmer equation as reported in (Tronconi et al. 2015).

Results and discussion

Structural and molecular docking analysis of Arabidopsis NADP-ME2

To better understand the structure–function relationship of NADP-ME2, we generated a three-dimensional (3D) model of this enzyme. The selection of the template was done considering enzymes with reported fumarate activation, known crystal structure and sequence identity. The only plant MEs with known crystal structures are from maize and sorghum (Alvarez et al. 2019), but both lack fumarate regulation (Detarsio et al. 2007; Saigo et al. 2013). Thus, the human isoform HsmNAD(P)-ME, which shares a 45.2% of amino acid identity and was crystallized in the presence of malate and fumarate, was selected as a template (PDB ID 1PJ2; (Tao et al. 2003); Fig. S1). As the first 44 amino acids of NADP-ME2 are absent in the human enzyme (Fig. S1), their 3D structure was constructed by de novo modeling. Stereochemical validation of the overall structure by the analysis of the Ramachandran plot, showed 96.2% of the residues in favored regions, 2.6% in allowed regions and only 1.2% in outlier regions. None of the outlier residues (Q145, T355, L400, K408, P409, K461, and R509) were present in the active or allosteric sites predicted in the model or in the N-terminal region.

The analysis of the final 3D model showed that NADP-ME2 monomeric structure could be divided into similar domains (A–D) as those previously described for HsmNAD(P)-ME (Fig. 1a; Chang and Tong 2003). The structures of domains B, C and D were conserved with regard to the template. Thus, Domain B is composed of two segments (residues 155–301 and 489–560) with a five stranded parallel β-sheet (βB1 through βB5) flanked by helices on both sides (αB1 through αB8). The active site located in the domain C (302–488) is defined by a NADP-binding Rossmann fold with the dinucleotide-binding signature

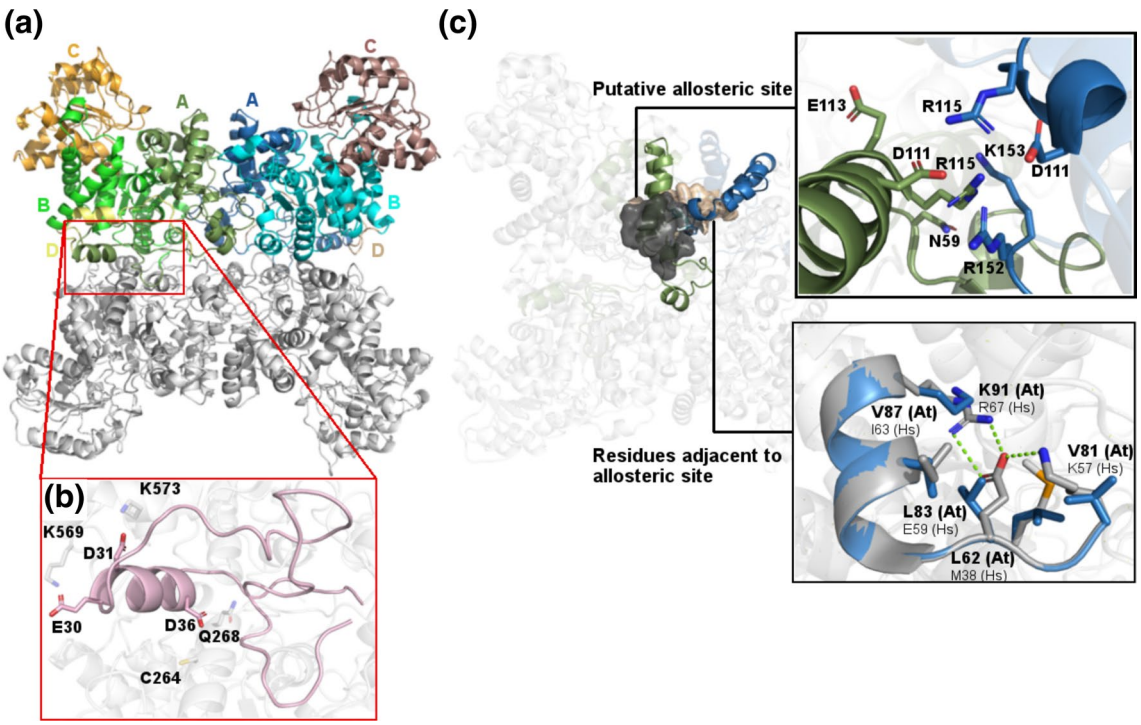

Fig. 1 NADP-ME2 model. **a** Cartoon representation of NADP-ME2 tetramer showing the dimers of dimers model. The four domains present are highlighted. **b** N-terminal chain containing conserved residues that could be involved in the tetramer stabilization. **c** Dimer interface between monomers 1 and 2, with a detailed view of allosteric and adjacent allosteric surfaces, highlighting the involved residues. The interaction pattern (green) of the adjacent allosteric residues in HsmNAD(P) (gray) are absent in *A. thaliana* NADP-ME2 (blue)

motif located between βC1 and αC2 (335-GAGEAG-340), as well as the malate binding site (Fig. 1a). Domain D (561–588) contains one α-helix followed by a long tail structure that protrudes away from the rest of the monomer (Fig. 1a). This C-terminal region is 18 residues shorter than in HsmNAD(P)-ME (Fig. S1), where some key residues are involved in the tetrameric conformation (Chang et al. 2007; Hsieh et al. 2009a; Murugan and Hung 2012).

The main differences between NADP-ME2 model and HsmNAD(P)-ME structure were found in domain A (residues 1–154). Firstly, it can be highlighted the presence of eight helices (αA1–αA8) in contrast with the six helices described for the human enzyme (Fig. 1a; (Chang and Tong 2003)). Secondly, the arrangement of the first 28 amino acids, likely as a loop, could provide additional connections between both dimers that conform the tetramer (Fig. 1a and b). Finally, it can be distinguished the presence of an α-helix between amino acids 29–38, in which residues E30, D31 and D36, could interact with residues C264, Q268, K569 and K573 of the other dimer and contribute to the protein stability (Fig. 1b).

In addition, NADP-ME2 domain A is predicted to form an allosteric site in the dimer interface analogous to the one found in HsmNAD(P)-ME (Fig. 1c; Yang et al. 2002a). The binding of fumarate to this site is responsible for the activation of the catalysis in both enzymes (Yang et al. 2002a; Gerrard Wheeler et al. 2008). From the four residues associated with fumarate binding to this site described for the human enzyme (Yang et al. 2002a; Hung et al. 2005; Hsieh et al. 2009b; Fig. S1), only two are conserved in NADP-ME2: R115 and D126, suggesting differences in the binding mode between these two enzymes. To further analyze the particularities of this site, molecular docking studies of NADP-ME2 wild-type and two mutant forms were performed. Interestingly, the best docking results for the parental and the mutant proteins were obtained with the side chains of the residues in the same orientation as in HsmNAD(P)-ME bound to fumarate (PDB ID 1PJ2 structure; Tao et al. 2003).

The interactions of fumarate and other possible ligands with the allosteric site of NADP-ME2 were studied (Fig. 2). Ionic interactions between each carboxylate of fumarate and amino acid side chains were detected: one with the protonated amine of K91 (d = 2.8 Å) and the other with the guanidine group of R115 (d = 2.9 Å; Fig. 2a). Both K91 and R115 residues are also conserved among many other malic enzymes that are insensitive to fumarate, therefore, additional structural determinants need to be present for fumarate regulation to occur (Chang and Tong 2003; Gerrard

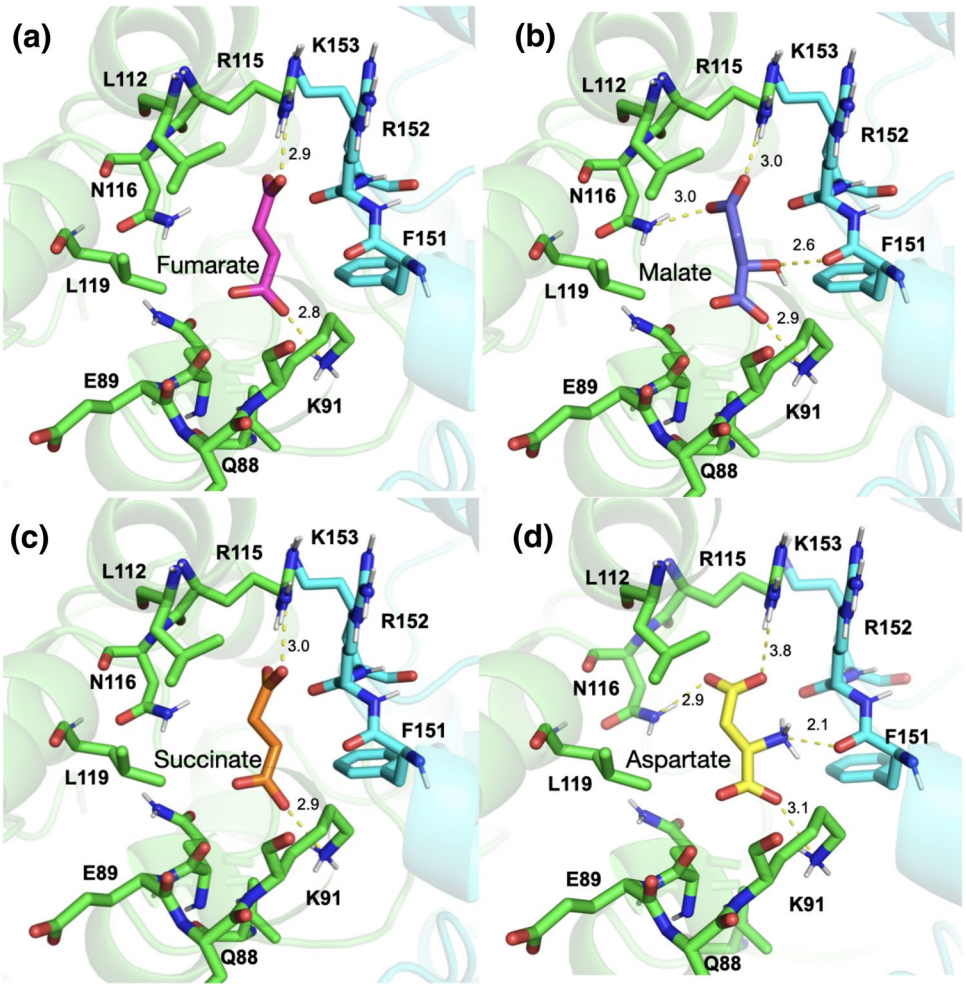

Fig. 2 Allosteric site of NADP-ME2 with fumarate (**a**), malate (**b**), succinate (**c**) and aspartate (**d**). The ligand interactions obtained by docking analysis are shown. The residues which directly interact with the ligands are displayed in green and cyan sticks and electrostatic interactions are represented as yellow dashed lines

Wheeler et al. 2009). On the other hand, when malate was evaluated as a possible ligand of the allosteric site, the docking analysis revealed that the substrate could also fit into fumarate's pocket and interact in a slightly different orientation (Fig. 2b). While the interactions with K91 and R115 were maintained, the C4 carboxylate group of malate also presented a ion–dipole interaction with the amide of N116 side chain (d = 3.0 Å) and an additional hydrogen bond between hydroxyl group of malate and the carbonyl of F151 (d = 2.6 Å, Fig. 2b). Thus, based on the results provided by the molecular docking, both malate and fumarate could bind to the allosteric site of NADP-ME2. Malate binding to this site could explain the sigmoidal response of NADP-ME2 with respect to this substrate (Arias et al. 2013) supporting a homotropic regulation hypothesis. Besides, the competence for the allosteric site could explain why the presence of fumarate reduces the sigmoidal behavior of the enzyme with respect to malate (Arias et al. 2013). Site occupancy by fumarate would disable the malate binding to the allosteric site and the enzyme exhibits a non-malate-regulated hyperbolic kinetics. Finally, the importance of the interaction with R115 at the allosteric site for both ligands is reflected in the loss of fumarate activation and malate hyperbolic behavior observed in ME2-R115A mutant (Table 1; Arias et al. 2013).

Succinate and aspartate, activators of NADP-ME2 reaction, were evaluated as possible ligands of the allosteric site. While succinate binding resembled fumarate positioning and interactions, showing ionic interactions with K91 and R115; aspartate binding seemed similar to malate, showing as well, the interactions with N116 and F151 (Fig. 2c and d). These results indicated that the structural similarity of these compounds allowed them to act as regulators of NADP-ME2 probably using the same allosteric binding site.

Docking analysis of fumarate within ME2-R115A allosteric site suggests a major shift in the orientation of the ligand (Fig. 3a and b). The interaction between fumarate and R115 observed in the wild-type protein was replaced by two new ion–dipole interactions between its carboxylate group and the guanidine group of R152 residue (d = 2.8 and 3.1 Å; Fig. 3a and b), maintaining the ionic interaction with K91 (d = 3.5 Å). This alteration in fumarate binding could explain previous kinetic studies that showed that ME2-R115A activity was not induced by this metabolite (Gerrard Wheeler et al. 2008; Arias et al. 2013).

Table 1 Kinetic parameters of the ME2-L62W in the absence of fumarate

	NADP-ME2	NADP-ME2-R115A	NADP-ME2-L62W
k_{cat} (s^{-1})	324 ± 29	234 ± 11	360 ± 30
$S_{0.5}$ NADP (mM)	0.072 ± 0.007	0.050 ± 0.002	6.1 ± 0.6
n_H NADP	1.3 ± 0.1	1.1 ± 0.2	0.9 ± 0.1
$S_{0.5}$ malate (mM)	3.3 ± 0.4	2.4 ± 0.2	18 ± 3[a]
n_H malate	2.1 ± 0.2	1.0 ± 0.1	1.1 ± 0.1

Indicated parameters are the average of three different experiments ± SD. For k_{cat}, a 65 kDa monomeric molecular mass was used. NADP-ME2 and ME2-R115A values were previously obtained (Gerrard et al. 2005, 2008; Arias et al. 2013) and included for comparison

[a]$S_{0.5}$ apparent determined at subsaturant concentration of NADP (1.5 mM)

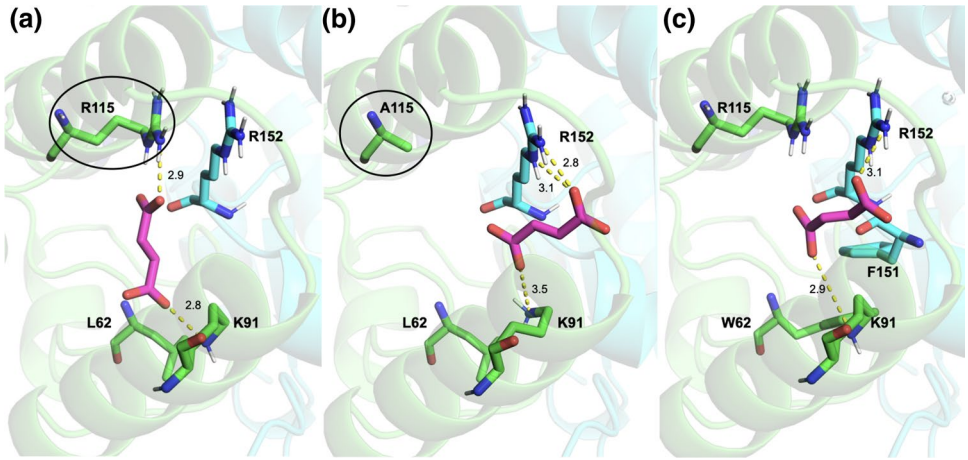

Fig. 3 Binding mode of fumarate at the allosteric site in NADP-ME2 (**a**), ME2-R115A (**b**) and ME2-L62W (**c**). Fumarate is displayed in pink sticks, the residues which directly interact with the ligands are displayed in green sticks and electrostatic interactions are represented as yellow dashed lines

In the human enzyme, ionic interactions between the residues K57-E59-R67, located in the surroundings of the allosteric site, were found to be responsible for stabilization of vicinal motifs and contribute to fumarate binding (Yang et al. 2002a; Hsieh et al. 2009b). In NADP-ME2, instead of charged residues, in the second sphere of the allosteric site there is a cluster of hydrophobic residues. Non conserved substitutions, regarding the residues in the human enzyme, such as: K57 to V81, E59 to L83 and M38 to L62 (Fig. 1c, panel below; Fig. S1) were found as part of the site's close environment. The importance of this region in the allosteric regulation was further investigated by the analysis of the 3D model of NADP-ME2 in which the leucine in position 62 was replaced by a tryptophan (ME2-L62W). This substitution preserves the hydrophobic pattern but creates a structural alteration due to the bigger volume of the tryptophan side chain. In the analysis of the model, no clashes were observed, suggesting that this mutation did not introduce a strong perturbation on the overall protein structure. Indeed, the substitution induced more rigidity in this region since W62 interacts through π-π stacking with F151 of about 3.7 Å and hydrophobic interactions with side chains of P79, V81 and L83 (Fig. 4). In addition, docking analysis of ME2-L62W predicted that despite the presence

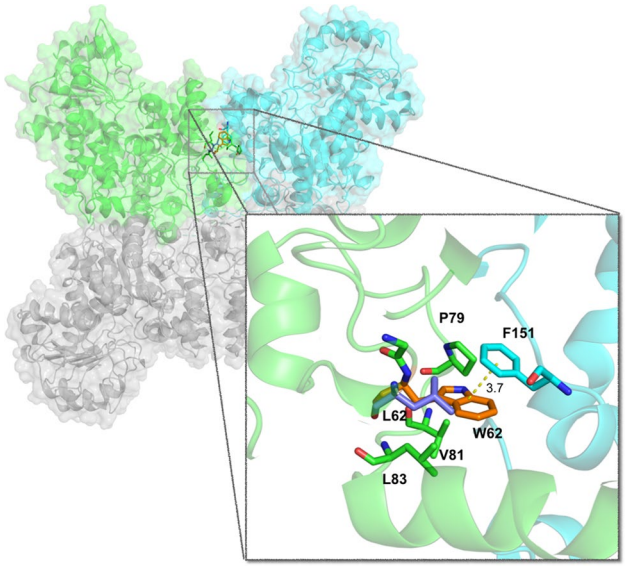

Fig. 4 Effect of L62W mutation on NADP-ME2 allosteric site. Superimposed view of leucine (in purple) and tryptophan (in orange) at position 62. The residues which directly interact with W62 are displayed in green sticks

of R115, fumarate binds to this mutant in a similar manner than it did to ME2-R115A (Fig. 3c). While no interaction with R115 was detected, it formed one new ion–dipole with R152 (d = 3.1 Å) and kept the ionic interaction with K91 (d = 2.9 Å). These new interactions possibly hinder electrostatic features of this site and affect the regulatory responsiveness of the enzyme. These data suggest a different mechanism by which residues surrounding the allosteric site participate in fumarate binding to NADP-ME2 in comparison to the previously described for HsmNAD(P)-ME.

Kinetic and structural characterization of NADP-ME2-L62W

To evaluate the possible conformational role of L62, we replaced this residue by site-directed mutagenesis generating the ME2-L62W protein. Recombinant expression and purification was achieved at high yield and purity (Fig. S2a). ME2-L62W showed no changes in the quaternary structure, as it is still able to form tetramers as well as the parental NADP-ME2 (Fig. S2b and c). Besides, we did not observe substantial differences in ellipticity in circular dichroism assays (Fig. S2d). These results confirm that the mutation does not produce a severe alteration in the native structure of the enzyme.

Then, we determined the kinetic parameters of ME2-L62W to evaluate if the general performance was affected by the substitution. In the mutant, the $S_{0.5}$ values for NADP and malate were 84.7 and 5.5 times higher than the values for the parental NADP-ME2 (Table 1). Thus, although the mutation is located near the allosteric site, away from the active site, both substrate affinities were severely decreased, which results interesting considering that fumarate activates NADP-ME2 by increasing its affinity for both substrates (Arias et al. 2013). Nevertheless, no important change was observed in the catalytic constant (k_{cat}; Table 1). Finally, for comparison, it is important to mention that the kinetic parameters from ME2-R115A did not differ from those of NADP-ME2 (Table 1; Gerrard Wheeler et al. 2008).

Furthermore, while NADP-ME2 showed a sigmoidal kinetics for malate, ME2-L62W exhibited a hyperbolic response ($n_H = 1.1$; Table 1). We also observed this loss of sigmoidal behaviour in ME2-R115A (Arias et al. 2013). These results are in agreement with the predicted malate binding to the NADP-ME2 allosteric site (Fig. 2b) and indicated essential roles for R115 and L62 residues in the substrate regulation. We further analyzed this mechanism by fluorescence titration assays. The proteins presented a heterogeneous population of tryptophan residues differing in their capacity to be quenched by malate. For NADP-ME2, a biphasic curve resulting in two linear segments was obtained (Fig. 5a). These results are consistent with malate binding to two sites with different affinity, possibly the active ($K_d = 1$ mM) and the allosteric ($K_d = 131$ mM) sites (Fig. 5a). Data representation for ME2-L62W was linear suggesting that malate in this enzyme is able to quench tryptophan residues from only one of the two populations (Fig. 5b). The K_d value obtained ($K_d = 10$ mM) corresponds to the affinity of ME2-L62W active site by malate in the absence of NADP. Thus, these results not only confirm that malate is able to bind to two sites in the NADP-ME2 but also that the L62W substitution affects its affinity for the active site and its binding to the allosteric site. In agreement with the kinetic results (Table 1), we observed a similar linear quenching pattern for ME2-R115A (Fig. 5c).

The activity of ME2-L62W was also evaluated in the presence of fumarate. In order to assess simultaneously the two possible types of effects of the fumarate in the enzyme's kinetics (V-type of K-type), the measurements were performed using subsaturating level of both substrates (equal to $S_{0.5}$ values for NADP and malate). In contrast to the strong activation effect of fumarate in NADP-ME2 (Arias et al.

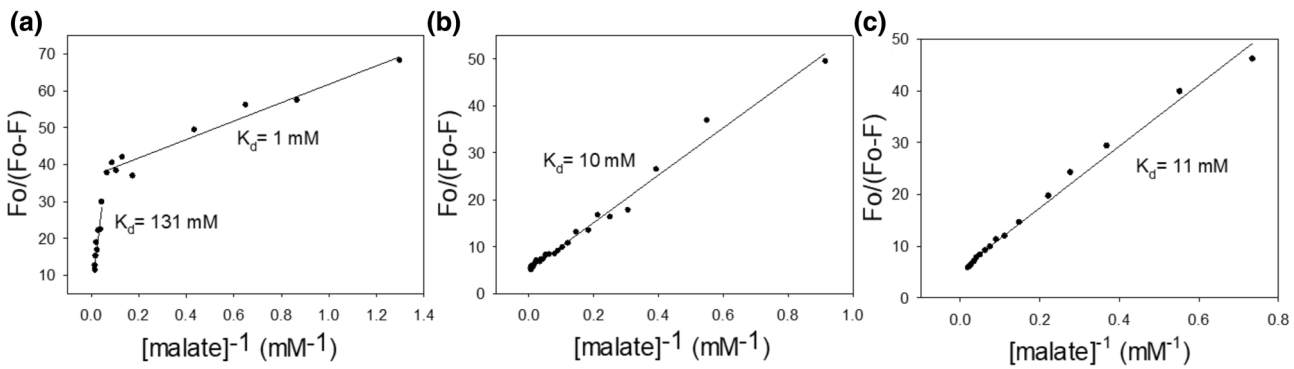

Fig. 5 Quenching fluorescence for NADP-ME2 and mutant forms. Modified Stern–Volmer representations of quenching by malate for NADP-ME2 (**a**), ME2-L62W (**b**) and ME2-R115A (**c**). The excitation wavelength was set at 295 nm and the fluorescence was recorded at 344 nm. Fo and F are the fluorescence of the enzyme alone or in the presence of quencher, respectively. The dissociation constants obtained are indicated. Typical results are shown from three independent determinations

2013), this metabolite was not able to activate the mutant (Fig. 6a). Fumarate, however, inhibited ME2-L62W activity up to 30% (at 25 mM), possibly competing with malate substrate for the active site, as it was observed for ME2-R115A (Arias et al. 2013). In both mutants, as shown by docking analysis, fumarate binding to the allosteric site was predicted to be severely affected, acquiring an altered orientation in the space and interacting with different residues from the site (Fig. 3). To complement the analysis, we further investigated fumarate binding to ME2-L62W by urea-induced denaturation assays. In the absence of fumarate, the enzyme was stable up to 1.5 M urea, leading to a partial inactivation at concentrations higher than 2 M (Fig. 6b). In the presence of fumarate, instead observing the protective effects that ligands usually provoke in the enzyme stability, ME2-L62W activity was significantly decreased above 0.5 M urea (Fig. 6b). Such a destabilizing effect was also observed in ME2-R115A, less pronounced and at higher concentrations of the denaturing agent (Arias et al. 2013). It should be noted that fumarate protected the parental enzyme from denaturation, retaining more than 70% of the enzyme activity even after treatments with 3 M urea (Arias et al. 2013). Finally, these results suggest that the abnormal binding of fumarate to ME2-L62W allosteric site, destabilizes the enzyme and prevents the transmission of the activation signal to the active site.

Prediction of NADP-ME2 functional dynamics

To get further insights into the allosteric regulation of this enzyme, we studied the protein functional dynamics by means of normal mode analysis (NMA). NMA is a well-established method to infer the main protein motions, starting from a single structure and expressing the concerted motions as a set of collective variables (Brooks and Karplus 1985). Using the structural model of NADP-ME2 (Fig. 1), we observed that the highest amplitude mode predicted, describing the most functionally relevant motion, corresponds to a dimer-dimer twisting motion (Fig. 7a; Video 1). This movement has been described before as a rigid-body shift of domains A and B in HsmNAD(P)-ME, which changes the tetramer reorganization and is related to enzyme activation (Chang and Tong 2003). The hinge regions associated with this mode, responsible for creating the conformational change, are highlighted by warmer colors (Fig. 7b). They are located at the junction point between protomers, around the N-terminal segment (residues 60–80), extending through the allosteric site till the active site. Very interestingly, the dimer-twisting motion described here is predicted to originate close to the L62 residue, which could explain how the L62W substitution affected substrate affinities in the active site far away from where the mutation is located. Thus, in NADP-ME2 the allosteric signal originate in this N-terminal region, causing conformational changes along the enzyme structure that would lead to the enzymatic activation. Thus, L62W mutation would distort the allosteric site displacing the equilibrium to a lower affinity catalytic state. This could be explained by the existence of two main conformations for NADP-ME2 according to the MWC allosteric model (Monod et al. 1965) which is in concordance to our results of docking, kinetics, fluorescence and urea assays described above. Altogether, our data pointed to a complex connection between tetramer assembly, binding site affinity and, allosteric activation, and a role in it for the N-terminal segment of NADP-ME2.

The complexity that state transitions or conformational changes can reach in ME was shown in the model suggested by crystallographic structures for the human malic enzyme (Chang and Tong 2003). In the case of NADP-ME2, the shifts between different conformational states in the presence of specific combinations of its ligands needs to be further studied by crystallographic structures of parental and

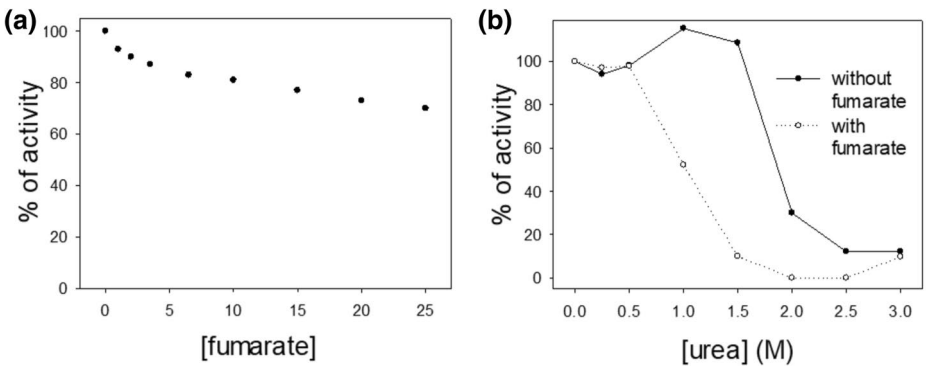

Fig. 6 Activity assays in the presence of fumarate. **a**) % of activity for ME2-L62W at different fumarate levels relative to the activity measured in the absence of it. The substrate concentrations used were 6 mM NADP and 18 mM malate. **b** Residual activity of ME2-L62W after incubation with different urea concentrations in the absence or presence of 20 mM fumarate. Typical results are shown from three independent determinations

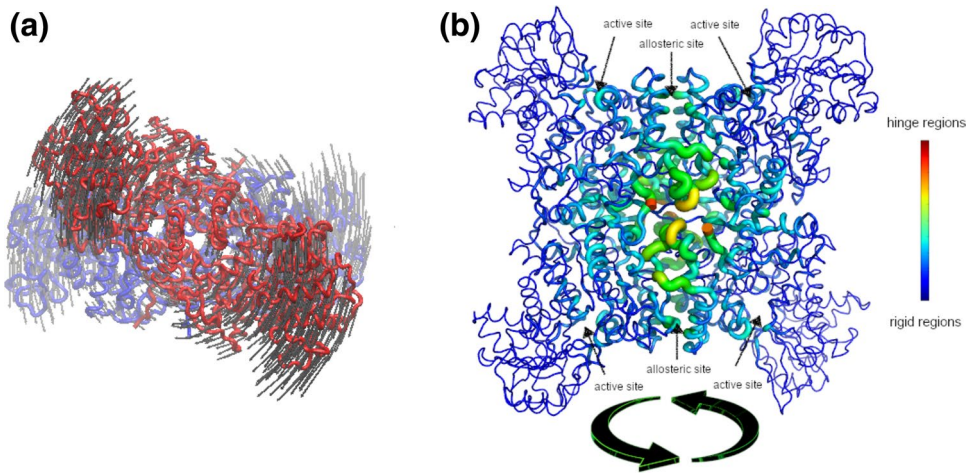

Fig. 7 Normal mode analysis of Arabidopsis NADP-ME2. **a** Dimer-twisting motion predicted as normal mode 1. One dimer is colored in red and the other in blue. The motion is highlighted by grey arrows. **b** Hinge regions in the dimer-twisting motion. The tetramer is observed from a different perspective than (**a**), with both dimers in the front plane, the first up and the second down. The allosteric and active sites are marked. A tubular representation is used for the protein backbone, with a bigger diameter together with warmer colors for regions acting as hinges. The motion is represented by curved arrows

its mutants versions. However, our data provides insights of the conformational changes that takes place after the correct binding of a ligand into the fumarate binding site as well as information of the regulatory properties of the system.

Concluding remarks

Malic enzymes (ME) isoforms throughout the different kingdoms present different biochemical properties, which would correlate with the ability of the proteins to fulfill specific metabolic functions. The precise identification of these differences in relation to the minimal primary structure changes is important for ME engineering. Allosteric regulations allow enzymes to rapidly and widely tune its catalytic activity in response to small changes in the concentration of its effectors. In this work, we performed a detailed study of the fumarate allosteric site of NADP-ME2, predicting that the binding of other regulators such as succinate, aspartate and even its own substrate malate is possible. In vivo this extended allosteric modulation would provide NADP-ME2 a broader sensing capacity of the cell status, combining stimulus from organic acid with amino acids to better respond to each of its diverse functions. The studies here reported revealed that the L62W substitution provokes an altered binding of fumarate that induces an unfavorable environment near the allosteric site, which is then transmitted to the active site, and culminates in reduced substrate affinities, inability of the mutant to be activated by fumarate and an increased enzyme instability, without affecting the global protein structure. In overall, we demonstrated the importance of L62 and other surrounding residues constituting the second sphere adjacent to NADP-ME2 allosteric site in the transmission of regulatory signals into the enzyme.

Supplementary Information The online version contains supplementary material available at https://doi.org/10.1007/s11103-021-01176-2.

Acknowledgements We thank Dra. Ana Bortolotti for her help with the use of the fluorometer and the IBR Institute for lending us this equipment. A MCGW, MFD and CEA belong to the Researcher Career of National Council of Scientific and Technical Research (CONICET); CLA participated as a fellow of the same institution. AMTS and CRR thanks Fundação Carlos Chagas Filho de Amparo à Pesquisa do Estado do Rio de Janeiro (FAPERJ).

Author contributions CEA conceived and led the project and together with MCGW and MFD designed and analyzed the experimental assays. CEA, CLA and MCGW designed the mutants and performed the kinetic and structural experiments. NCD performed and analyzed the NMA. JFRM and AMTS performed and analyzed the model structures and docking studies. CRR and AMTS supported all the computational work. All authors contributed to the writing of the manuscript and approved it.

Funding This work was supported by CONICET and National Agency for Promotion of Science and Technology. This study was financed in part by the Coordenação de Aperfeiçoamento de Pessoal de Nível Superior – Brasil (CAPES) – Finance Code 001 (JFRM). This work was supported in part by a grant from Fundação Carlos Chagas Filho de Amparo à Pesquisa do Estado do Rio de Janeiro (FAPERJ), Number E-26/203.179/2016.

References

Alvarez CE, Trajtenberg F, Larrieux N, Saigo M, Golic A, Andreo CS, Hogenhout SA, Mussi MA, Drincovich MF, Buschiazzo A (2018) The crystal structure of the malic enzyme from *Candidatus*

Phytoplasma reveals the minimal structural determinants for a malic enzyme. Acta Crystallogr Sect D 74:332–340. https://doi.org/10.1107/S2059798318002759

Alvarez CE, Bovdilova A, Höppner A, Wolff CC, Saigo M, Trajtenberg F, Zhang T, Buschiazzo A, Nagel-Steger L, Drincovich MF, Lercher MJ, Maurino VG (2019) Molecular adaptations of NADP-malic enzyme for its function in C_4 photosynthesis in grasses. Nat Plants 5:755–765. https://doi.org/10.1038/s41477-019-0451-7

Araújo WL, Nunes-Nesi A, Fernie AR (2011) Fumarate: multiple functions of a simple metabolite. Phytochemistry 72:838–843. https://doi.org/10.1016/j.phytochem.2011.02.028

Arias CL, Andreo CS, Drincovich MF, Gerrard Wheeler MC (2013) Fumarate and cytosolic pH as modulators of the synthesis or consumption of C(4) organic acids through NADP-malic enzyme in *Arabidopsis thaliana*. Plant Mol Biol 81:297–307. https://doi.org/10.1007/s11103-012-9999-6

Badia MB, Mans R, Lis AV, Tronconi MA, Arias CL, Maurino VG, Andreo CS, Drincovich MF, van Maris AJA, Gerrard Wheeler MC (2017) Specific *Arabidopsis thaliana* malic enzyme isoforms can provide anaplerotic pyruvate carboxylation function in *Saccharomyces cerevisiae*. FEBS J 284:654–665. https://doi.org/10.1111/febs.14013

Bakan A, Meireles LM, Bahar I (2011) ProDy: protein dynamics inferred from theory and experiments. Bioinformatics 27:1575–1577. https://doi.org/10.1093/bioinformatics/btr168

Berman HM, Bhat TN, Bourne PE, Feng Z, Gilliland G, Weissig H, Westbrook J (2000) The Protein Data Bank and the challenge of structural genomics. Nat Struct Biol 7:957–959. https://doi.org/10.1038/80734

Brooks B, Karplus M (1985) Normal modes for specific motions of macromolecules: application to the hinge-bending mode of lysozyme. Proc Natl Acad Sci USA 82:4995–4999. https://doi.org/10.1073/pnas.82.15.4995

Brown NJ, Palmer BG, Stanley S, Hajaji H, Janacek SH, Astley HM, Parsley K, Kajala K, Quick WP, Trenkamp S, Fernie AR, Maurini VG, Hibberd JM (2010) C_4 acid decarboxylases required for C_4 photosynthesis are active in the mid-vein of the C_3 species *Arabidopsis thaliana*, and are important in sugar and amino acid metabolism. Plant J 61:122–133. https://doi.org/10.1111/j.1365-313X.2009.04040.x

Chang G, Tong L (2003) Structure and function of malic enzymes, a new class of oxidative decarboxylases. Biochemistry 42:12721–12733. https://doi.org/10.1021/bi035251

Chang H-C, Chen L-Y, Lu Y-H, Li M-Y, Chen Y-H, Lin C-H, Chang G-G (2007) Metal ions stabilize a dimeric molten globule state between the open and closed forms of malic enzyme. Biophys J 93:3977–3988. https://doi.org/10.1529/biophysj.107.111385

Coleman DE, Rao GSJ, Goldsmith EJ, Cook PF, Harris BG (2002) Crystal structure of the malic enzyme from *Ascaris suum* complexed with nicotinamide adenine dinucleotide at 2.3 Å resolution. Biochemistry 41:6928–6938. https://doi.org/10.1021/bi0255120

Detarsio E, Gerrard Wheeler MC, Campos Bermúdez VA, Andreo CS, Drincovich MF (2003) Maize C_4 NADP-malic enzyme. Expression in *Escherichia coli* and characterization of site-directed mutants at the putative nucleoside-binding sites. J Biol Chem 278:13757–13764. https://doi.org/10.1074/jbc.M212530200

Detarsio E, Alvarez CE, Saigo M, Andreo CS, Drincovich MF (2007) Identification of domains involved in tetramerization and malate inhibition of maize C_4-NADP-malic enzyme. J Biol Chem 282:6053–6060. https://doi.org/10.1074/jbc.M609436200

Dolinsky TJ, Nielsen JE, McCammon JA, Baker NA (2004) PDB2PQR: an automated pipeline for the setup of Poisson–Boltzmann electrostatics calculations. Nucleic Acids Res 32:665–667. https://doi.org/10.1093/nar/gkh381

Drincovich MF, Lara MV, Andreo CS, Maurino VG (2010) C_4 decarboxylases: different solutions for the same biochemical problem, the provision of CO_2 to rubisco in the bundle sheath cells. In: Raghavendra A, Sage R (eds) C_4 photosynthesis and related CO_2 concentrating mechanisms. Advances in photosynthesis and respiration. Springer, Dordrecht, pp 277–300

Eyal E, Lum G, Bahar I (2015) The anisotropic network model web server at 2015 (ANM 2.0). Bioinformatics 31:1487–1489. https://doi.org/10.1093/bioinformatics/btu847

Fernie AR, Martinoia E (2009) Malate. Jack of all trades or master of a few? Phytochemistry 70:828–832. https://doi.org/10.1016/j.phytochem.2009.04.023

Gerrard Wheeler MC, Tronconi MA, Drincovich MF, Andreo CS, Flügge UI, Maurino VG (2005) A comprehensive analysis of the NADP-malic enzyme gene family of Arabidopsis. Plant Physiol 139:39–51. https://doi.org/10.1104/pp.105.065953

Gerrard Wheeler MC, Arias CL, Tronconi MA, Maurino VG, Andreo CS, Drincovitch MF (2008) *Arabidopsis thaliana* NADP-malic enzyme isoforms: high degree of identity but clearly distinct properties. Plant Mol Biol 67:231–242. https://doi.org/10.1007/s11103-008-9313-9

Gerrard Wheeler MC, Arias CL, Maurino VG, Andreo CS, Drincovich MF (2009) Identification of domains involved in the allosteric regulation of cytosolic *Arabidopsis thaliana* NADP-malic enzymes. FEBS J 276:5665–5677. https://doi.org/10.1111/j.1742-4658.2009.07258.x

Grant BJ, Rodrigues APC, ElSawy KM, McCammon JA, Caves LSD (2006) Bio3d: an R package for the comparative analysis of protein structures. Bioinformatics 22:2695–2696. https://doi.org/10.1093/bioinformatics/btl461

Hsieh J-Y, Chen S-H, Hung H-C (2009a) Functional roles of the tetramer organization of malic enzyme. J Biol Chem 284:18096–18105. https://doi.org/10.1074/jbc.M109.005082

Hsieh J-Y, Chiang Y-H, Chang K-Y, Hung H-C (2009b) Functional role of fumarate site Glu59 involved in allosteric regulation and subunit-subunit interaction of human mitochondrial NAD(P)+-dependent malic enzyme. FEBS J 276:983–994. https://doi.org/10.1111/j.1742-4658.2008.06834.x

Hsieh J-Y, Shih W-T, Kuo Y-H, Liu G-Y, Hung H-C (2019) Functional roles of metabolic intermediates in regulating the human mitochondrial NAD(P)+-dependent malic enzyme. Sci Rep 9:1–14. https://doi.org/10.1038/s41598-019-45282-0

Humphrey W, Dalk A, Schulten K (1996) VMD: visual molecular dynamics. J Mol Graph 14(33–38):27–28. https://doi.org/10.1016/0263-7855(96)00018-5

Hung HC, Kuo MW, Chang GG, Liu GY (2005) Characterization of the functional role of allosteric site residue Asp 102 in the regulatory mechanism of human mitochondrial NAD(P)+-dependent malate dehydrogenase (malic enzyme). Biochem J 392:39–45. https://doi.org/10.1042/BJ20050641

Laskowski RA, MacArthur MW, Moss DS, Thornton JM (1993) PROCHECK: a program to check the stereochemical quality of protein structures. J Appl Crystallogr 26:283–291. https://doi.org/10.1107/s0021889892009944

Maurino VG, Engqvist MK (2015) 2-Hydroxy acids in plant metabolism. Arabidopsis Book 13:e0182. https://doi.org/10.1199/tab.0182

Monod J, Wyman J, Changeux J-P (1965) On the nature of allosteric transitions: a plausible model. J Mol Biol 12:88–118. https://doi.org/10.1016/S0022-2836(65)80285-6

Morris GM, Huey R, Lindstrom W, Sanner MF, Belew RK, Goodsell DS, Olson AJ (2009) AutoDock4 and AutoDockTools4: automated docking with selective receptor flexibility. J Comput Chem 30:2785–2791. https://doi.org/10.1002/jcc.21256

Murugan S, Hung H (2012) Biophysical characterization of the dimer and tetramer Interface interactions of the human cytosolic malic enzyme. PLoS ONE 7:1–11. https://doi.org/10.1371/journal.pone.0050143

Pettersen EF, Goddard TD, Huang CC, Couch GS, Greenblatt DM, Meng EC, Ferrin TE (2004) UCSF Chimera - a visualization system for exploratory research and analysis. J Comput Chem 25:1605–1612. https://doi.org/10.1002/jcc.20084

Rao GSJ, Coleman DE, Karsten WE, Cook PF, Harris BG (2003) Crystallographic studies on *Ascaris suum* NAD-malic enzyme bound to reduced cofactor and identification of an effector site. J Biol Chem 278:38051–38058. https://doi.org/10.1074/jbc.M305145200

Saigo M, Alvarez CE, Andreo CS, Drincovich MF (2013) Plastidial NADP-malic enzymes from grasses: unraveling the way to the C4 specific isoforms. Plant Physiol Biochem 63:39–48. https://doi.org/10.1016/j.plaphy.2012.11.009

Šali A, Blundell TL (1993) Comparative protein modelling by satisfaction of spatial restraints. J Mol Biol 234:779–815. https://doi.org/10.1006/jmbi.1993.1626

Tao X, Yang Z, Tong L (2003) Crystal structures of substrate complexes of malic enzyme and insights into the catalytic mechanism. Structure 11:1141–1150. https://doi.org/10.1016/S0969-2126(03)00168-0

Tronconi MA, Gerrard Wheeler MC, Martinatto A, Zubimendi JP, Andreo CS, Drincovich MF (2015) Allosteric substrate inhibition of Arabidopsis NAD-dependent malic enzyme 1 is released by fumarate. Phytochemistry 111:37–47. https://doi.org/10.1016/j.phytochem.2014.11.009

Tronconi MA, Andreo CS, Drincovich MF (2018) Chimeric structure of plant malic enzyme family: different evolutionary scenarios for NAD- and NADP-dependent isoforms. Front Plant Sci 9:1–15. https://doi.org/10.3389/fpls.2018.00565

Voll LM, Zell MB, Engelsdorf T, Saur A, Gerrard Wheeler MC, Drincovich MF, Weber APM, Maurino VG (2012) Loss of cytosolic NADP-malic enzyme 2 in Arabidopsis is associated with enhanced susceptibility towards *Colletotrichum higginsianum*. New Phytol 195:189–202. https://doi.org/10.1111/j.1469-8137.2012.04129.x

Xu Y, Bhargava G, Wu H, Loeber G, Tong L (1999) Crystal structure of human mitochondrial NAD (P) + -dependent malic enzyme : a new class of oxidative decarboxylases. Structure 7:877–889. https://doi.org/10.1016/S0969-2126(99)80115-4

Yang J, Zhang Y (2015) I-TASSER server: new development for protein structure and function predictions. Nucleic Acids Res 43:W174–W181. https://doi.org/10.1093/nar/gkv342

Yang Z, Lanks CW, Tong L (2002a) Molecular mechanism for the regulation of human mitochondrial NAD(P)+-dependent malic enzyme by ATP and fumarate. Structure 10:951–960. https://doi.org/10.1016/S0969-2126(02)00788-8

Yang Z, Zhang H, Hung HC, Kuo CC, Tsai LC, Yuan HS, Chou WY, Chang GG (2002b) Structural studies of the pigeon cytosolic NADP(+) -dependent malic enzyme. Protein Sci 11:332–341. https://doi.org/10.1110/ps.38002